Received: 24 June 2025 | Accepted: 17 January 2026

DOI: 10.1097/HC9.0000000000000928

ORIGINAL ARTICLE

OPEN

Single-cell profiling reveals hepatic monocyte-derived macrophages heterogeneity during steatotic liver disease

Haozhe Xu[1,2] | **Lu Yang**[3] | **Peiyang Fang**[1,2] | **Jie Sun**[1,2] | **Xinjie Zhong**[1,2] | **Wanqing Deng**[1,2] | **Siqi Li**[1,2] | **Longyang Zhou**[1,2] | **Jinguo Fan**[1,2] | **Dong Zhang**[1,2] | **Guangyong Sun**[1,2]

[1]Medical Research Center, Beijing Institute of Respiratory Medicine, Beijing Chao-Yang Hospital, Capital Medical University, Beijing, China

[2]Department of Gastroenterology, Beijing Chao-Yang Hospital, Capital Medical University, Beijing, China

[3]Department of General Surgery, Beijing Friendship Hospital, Capital Medical University, Beijing, China

Correspondence
Dong Zhang, 8 South GongTi Road, Beijing Chaoyang District, Beijing 100020, China.
Email: zhangd@ccmu.edu.cn

Guangyong Sun, 8 South GongTi Road, Beijing Chaoyang District, Beijing 100020, China.
Email: sungy@ccmu.edu.cn

Abstract

Background: Monocyte-derived macrophages (MoMFs) play key roles in liver inflammation and fibrogenesis, with their heterogeneity affecting metabolic dysfunction–associated steatotic liver disease (MASLD) progression. However, current therapeutic strategies targeting macrophage-mediated inflammation have shown limited clinical efficacy in MASLD.

Methods: We conducted single-cell RNA sequencing (scRNA-seq) of liver-infiltrating 7AAD$^-$CD45$^+$Ly6G$^-$CD11b^{hi}F4/80^{int} MoMFs from NCD-fed and MCD-fed mice. Monocle 2 and CellChat analyses explored developmental trajectories and intercellular interactions, respectively.

Results: Seven distinct clusters (c0–c6) with unique molecular signatures were identified. Beyond the classical CD206$^+$ M2-polarized MoMFs, we identified 2 distinct subsets: CCR3$^+$ (c3) MoMFs with enhanced pro-inflammatory and oxidative stress activities, and CCR7$^+$ (c4) MoMFs with specialized antigen-presenting capacity in MASLD mouse livers. Although CCR2$^+$ MoMFs are classically considered pro-inflammatory, our study revealed that the predominant CD14$^+$CCR2$^+$ (c0) MoMFs exhibit additional functional roles in fibrosis, lipid accumulation, and antigen presentation. Our pseudotime and in vitro data demonstrate that resident basal c1 MoMFs are phenotypically plastic, capable of acquiring CD14$^+$/CCR7$^+$ markers and

Abbreviations: BP, biological process; CDHFD, choline-deficient high-fat diet; Cholangio, cholangiocytes; Clec5a, C-type lectin domain family 5 member a; CDHFD, choline-deficient high-fat diet; DEGs, differentially expressed genes; EC, endothelial cell; F13a1, factor XIII A chain; Fn1, fibronectin 1; GO, Gene Ontology; Gpr84, G protein–coupled receptor 84; H2-Eb2, histocompatibility 2 class II antigen E beta 2; Hep, hepatocytes; H&E, Hematoxylin and Eosin; HFD, high-fat diet; Hp, haptoglobin; IL-1β, interleukin 1 beta; KC, Kupffer cell; Kdr, kinase insert domain receptor; KEGG, Kyoto Encyclopedia of Genes and Genomes; LAMs, lipid-associated macrophages; LPS, lipopolysaccharide; MASLD, metabolic dysfunction–associated steatotic liver disease; MASH, metabolic dysfunction–associated steatohepatitis; MCD, methionine/choline-deficient diet; Mmp8, matrix metallopeptidase 8; MoKCs, monocyte-derived Kupffer cells; MoMFs, monocyte-derived macrophages; Mono/Mac, monocytes/macrophages; Mrc1, mannose receptor C-type 1; NAS, NAFLD activity score; NCD, normal control diet; PCA, principal component analysis; Retnlg, resistin like gamma; ROS, reactive oxygen species; S100a10, S100 calcium binding protein A10; scRNA-seq, single-cell RNA sequencing; Sell, selectin L; Stab1, stabilin 1; TNFα, tumor necrosis factor alpha; Trem3, triggering receptor expressed on myeloid cells 3; Treml4, triggering receptor expressed on myeloid cells-like 4; UMAP, uniform manifold approximation and projection.

Haozhe Xu and Lu Yang share co-first authorship.

Supplemental Digital Content is available for this article. Direct URL citations are provided in the HTML and PDF versions of this article on the journal's website, www.hepcommjournal.com.

transitioning toward c0-like and c4-like states, implying a potential intrahepatic origin for these subsets in diet-induced steatohepatitis. Notably, these MoMFs subsets and their dynamic changes during disease progression were conserved between the mouse models and human MASLD samples.

Conclusions: Our study systematically characterized the heterogeneity and dynamic changes in intrahepatic MoMFs during MASLD progression. Resident c1 MoMFs are plastic and could be a local source for $CD14^+$/$CCR7^+$ subsets in MASLD without relying solely on bone marrow recruitment. These findings provide new insights into the therapeutic strategies that target macrophage-mediated inflammation in MASLD.

Keywords: CCR2, CCR3, CCR7, cell plasticity, MASLD, single-cell RNA sequencing

INTRODUCTION

Metabolic dysfunction–associated steatotic liver disease (MASLD), a progressive precursor to metabolic dysfunction–associated steatohepatitis (MASH), affects ~24% of the global population, posing a substantial health burden.[1–3] Immune dysregulation critically drives disease pathogenesis, wherein macrophages centrally coordinate disease progression.[4–6]

Hepatic macrophages comprise 2 distinct populations: tissue-resident Kupffer cells (KCs), which maintain liver homeostasis under physiological conditions, and recruited monocyte-derived macrophages (MoMFs), which exhibit remarkable functional plasticity and represent an important subset in liver immunology and pathology.[7–9] Macrophages play dynamic roles in liver disease progression, such as through M1/M2 polarization, lipid processing, and interactions with hepatic cells, critically influencing liver homeostasis and steatosis development.[6] The CCR2–CCL2 axis has been identified as a predominant chemotactic pathway for monocyte recruitment to the injured liver, with $CCR2^+$ monocytes constituting a significant proportion of infiltrating cells in experimental models of liver injury.[10] However, clinical trials targeting this pathway have yielded disappointing results, suggesting a more complex mechanism than initially proposed.[11]

Recent studies have identified specialized MoMFs populations, including $TREM2^+$ lipid-associated macrophages accumulating in response to lipid overload,[12,13] and $S100A4^+$ MoMFs involved in promoting liver fibrosis.[14] The emergence of these functionally distinct subpopulations highlights the remarkable heterogeneity within the MoMFs compartment that may not be effectively targeted by broad CCR2 inhibition strategies. With the emergence of single-cell RNA sequencing (scRNA-seq) technologies, there is now an opportunity to systematically characterize the heterogeneity of MoMFs throughout MASLD progression, potentially uncovering novel therapeutic targets and disease mechanisms.[15]

This study aims to elucidate the heterogeneity of liver MoMFs and their functions during the progression of MASLD using scRNA-seq. Through analysis of publicly available human MASLD datasets, we investigate whether these MoMFs subsets are conserved across species. Our findings seek to advance the understanding of MASLD pathogenesis and reveal potential therapeutic targets for modulating MoMF functions in liver disease.

METHODS

Animal studies

Weight-matched 8-week-old male C57BL/6 wild-type mice were purchased from the Jackson Laboratory (USA). Animals were randomly assigned to receive either a normal control diet (NCD) or one of the following: choline-deficient high-fat diet (CDHFD, D05010402, Research Diets), methionine/choline-deficient diet (MCD, H10401, Beijing HFK Bioscience), or high-fat diet (HFD, D12492, Research Diets). All procedures involving animals conformed to the approved guidelines for animal care and use and were conducted under the ethical approval granted by the Institutional Animal Care and Ethics Committee of Capital Medical University (IACUC approval number: AEEI-2023-282). The study is reported in accordance with the ARRIVE (Animals in Research: Reporting *In vivo* Experiments) guidelines.

Intrahepatic immune cell isolation and flow cytometry analysis

Intrahepatic immune cells were collected as previously described.[16] Cell surface markers were stained with fluorochrome-conjugated antibodies (30 min, 4 °C). For intracellular/nuclear antigens, cells were fixed and permeabilized before staining. To evaluate cytokine production, cells were stimulated with a cell activation cocktail (423304, BioLegend) for 4–6 hours at 37 °C before staining. Samples were analyzed on BD FACS Aria II (BD Biosciences), and data were analyzed using FlowJo software (Tree Star Inc.).

RNA extraction and quantitative real-time PCR (qRT-PCR)

Total RNA was obtained from liver tissue using TRIzol reagent (Invitrogen) and converted to cDNA via PrimeScript RT Master Mix (Takara). qRT-PCR was conducted on a 7500 Fast Real-time PCR System (Applied Biosystems) using SYBR Green Master Mix (Applied Biosystems). Gene expression was normalized to GAPDH and analyzed using the $2^{-\Delta\Delta Ct}$ method. The primer sequences are provided in Supplemental Table S1, http://links.lww.com/HC9/C280.

Single-cell RNA sequencing analysis

Intrahepatic MoMFs ($7AAD^{-}CD45^{+}Ly6G^{-}CD11b^{hi}F4/80^{int}$) from NCD-fed or MCD-fed mice (n = 2 per group) were processed using the 10x Genomics Chromium Single-Cell 3' platform (v3) for cDNA library construction. Sequencing was performed on an Illumina NovaSeq 6000 system, and raw FASTQ data were analyzed with Cell Ranger (v3.0.2) using the mm10 reference genome.

Count matrices were processed in R (v4.3.1) using Seurat (v4.9.9). Cells with mitochondrial gene expression below 20% and with more than 500 genes detected were retained for downstream analysis. B-cell clusters (identified by *Cd19* expression) and clusters containing < 70 cells were further excluded, resulting in 10,962 high-quality cells for downstream analyses.

Data were log-normalized (scale factor = 10,000) and scaled after regressing out mitochondrial gene expression. Highly variable features (top 2000) were identified using the "vst" method. Principal component analysis (PCA) was performed, and the first 30 principal components were used for downstream steps. UMAP was applied for dimensionality reduction (dims = 1:30), and a resolution of 0.15 was selected based on marker-gene expression coherence and biological interpretability. Cell clusters were manually annotated according to cluster-specific marker-gene profiles.

Cluster-specific marker genes were identified using the FindAllMarkers function (Wilcoxon rank-sum test, min.pct = 0.25, logfc.threshold = 0.25), retaining genes with an adjusted *p*-value < 0.05 after Bonferroni correction. Differential expression between dietary conditions within each MoMFs cluster was assessed with FindMarkers (Wilcoxon rank-sum test, min.pct = 0.25, logfc.threshold = 0). Genes with an adjusted *p*-value < 0.05 and $|\log_2 FC| > 0.25$ were considered significant. Functional enrichment analysis was performed with clusterProfiler (v4.8.3) using the compareCluster function for Gene Ontology (GO) (ont = "ALL", pool = TRUE) and Kyoto Encyclopedia of Genes and Genomes (KEGG) pathways.

Trajectory analysis

Differentiation trajectories were reconstructed using Monocle 2 (v2.30.0) for selected clusters (c0, c1, c4, c5). Ordering genes were identified by differential expression testing (*q*-value < 0.01) using differentialGeneTest. Trajectory inference used DDRTree dimensionality reduction (max_components = 2) with root_state = 4. All analyses used default parameters unless otherwise specified.

Cell communication analysis

Cell–cell communication networks were compared between normal and MASLD conditions using CellChat (v2.1.2) on human and mouse single-cell resolution datasets. Following cell annotation based on cluster-specific marker genes, normalized expression matrices and metadata were extracted from Seurat objects. Species-specific ligand–receptor databases were used for network inference. Communication probabilities were calculated via computeCommunProb and filtered for interactions (min.cells = 10), then aggregated at the pathway level with compute Commun Prob Pathway.

For comparison, CellChat objects from the NCD and MCD groups were merged using mergeCellChat. Differentially expressed ligand–receptor pairs were identified with identifyOverExpressedGenes (thresh.pc = 0.1, thresh.fc = 0.1, thresh.*P* = 1). Upregulated interactions were defined as ligand $\log_2$ fold-change > 0.2 for downstream analysis.

CCR7 and CCR2 targeted interventions in MCD-fed mice

For intervention studies targeting distinct MoMFs subsets in MCD-fed mice, the following reagents and protocols were employed. To target $CCR7^{+}$ MoMFs,

mice received twice-weekly intravenous (i.v.) injections of an anti-mouse CCR7 neutralizing antibody (MAB3477, R&D Systems) at 10 μg per mouse or an IgG2A isotype control (clone 4B12, R&D Systems).[17,18]

To target CCR2$^+$ MoMFs, mice were fed an MCD diet for 4 weeks. During the final 2 weeks, they received daily intraperitoneal (i.p.) injections of the CCR2 antagonist RS102895 (5 mg/kg, HY-18611A, MedChemExpress) or vehicle control.[19,20] RS102895 was prepared as a 25 mg/mL stock in DMSO and diluted to 1 mg/mL in a vehicle of 40% PEG300 (HY-Y0873, MedChemExpress), 5% Tween 80 (HY-Y1891, MedChemExpress), and 51% saline. The vehicle control contained 4% DMSO in the same formulation. Corresponding NCD-fed groups served as healthy controls in both intervention settings.

Statistical analysis

Data analysis was performed using GraphPad Prism 9.0 (GraphPad Software), with results expressed as mean ± SD. The Shapiro–Wilk test determined data normality. For normally distributed data, we applied the Student *t* test for 2-group comparisons and one-way ANOVA with appropriate post hoc testing for multiple groups. Non-normally distributed data were analyzed using the Mann–Whitney *U* test for 2 groups or the Kruskal–Wallis test followed by the Dunn post hoc test for multiple group comparisons. A 2-tailed *p*-value < 0.05 was considered statistically significant.

RESULTS

scRNA-seq delineates the remodeled landscape of MoMFs in MCD diet-induced murine livers

To explore the heterogeneity of liver MoMFs during steatohepatitis progression, we isolated 7AAD$^-$CD45$^+$Ly6G$^-$CD11b^{hi}F4/80^{int} cells from the livers of NCD and MCD-fed mice for scRNA-seq (Figure 1A and Supplemental Figure S1A, http://links.lww.com/HC9/C281). After quality control, uniform manifold approximation and projection (UMAP) analysis revealed 7 distinct clusters (c0–c6) annotated by specific marker genes (Figures 1B, C and Supplemental Figures S1B–D, http://links.lww.com/HC9/C281).

c0 exhibited high expression of coagulation factor XIII A chain (*F13a1*), haptoglobin (*Hp*), fibronectin 1 (*Fn1*), and CD14 antigen (*Cd14*), suggesting that the monocytes primarily originated from bone marrow and myeloid lineage cells (Figures 1D, E).[21,22] GO enrichment analysis revealed that this cluster is associated with various metabolic and inflammatory pathways, including lipid catabolism, reactive oxygen species (ROS) metabolism, and interleukin-1 production (Figure 1F). Notably, c0 emerged as the most abundant cluster in the MCD group and showed a marked increase compared with the NCD group, indicating its potential involvement in diet-induced steatohepatitis progression (Figure 1G). c1, which represents the predominant cluster in the NCD group, showed higher expression of ribosome-associated genes, defining it as a basal population (Figures 1D–G). The relative proportion of this cluster is substantially reduced in the MCD group (Figure 1G).

c2 expressed high levels of mannose receptor C-type 1 (*Mrc1*), kinase insert domain protein receptor (*Kdr*), and stabilin 1 (*Stab1*) (Figures 1D, E). GO analysis suggested that this cluster has anti-inflammatory functions, implying a role in maintaining liver homeostasis (Figure 1F).[23,24] The reduced proportion of c2 in MCD-fed mice may indicate impaired anti-inflammatory responses during diet-induced steatohepatitis progression (Figure 1G). Conversely, c3 displayed high expression of C-C motif chemokine receptor 3 (*Ccr3*) and resistin-like gamma (*Retnlg*), and GO analysis indicated a link to NF-κB pathway activation, suggesting a pro-inflammatory role (Figures 1D–F).[25,26] The increase in c3 proportion in the MCD group aligns with the inflammatory characteristics of the disease (Figure 1G). The antigen-presenting cluster 4 (*Ccr7*$^+$ and *Cd209a*$^+$) increased in MASLD, suggesting enhanced adaptive immune interactions (Figures 1D–G).[26,27] c5 and c6 showed distinct molecular signatures but minimal changes in proportion between groups. c5 was characterized by high expression of topoisomerase II alpha (*Top2a*) and antigen identified by monoclonal antibody Ki67 (*Mki67*), indicating proliferative activity (Figures 1D–G). c6 exhibited elevated expression of *Cd3d* and granzyme B (*Gzmb*), with GO analysis revealing associations with T cell functionality (Figures 1D–G).[28,29]

Collectively, these findings reveal a comprehensive remodeling of the hepatic MoMFs landscape, marked by a shift from homeostasis-sustaining populations to pro-inflammatory, metabolically active, and immune-interactive subsets during diet-induced steatohepatitis (Figures 1F, G).

Lipid overload drives mitochondrial dysfunction and apoptosis in CD206$^+$ (c2) MoMFs during MASLD progression

To elucidate the mechanisms underlying the significant alterations in MoMFs subsets distributions during MASLD progression, we conducted a comprehensive analysis of each cluster. Feature plots revealed high expression of anti-inflammatory *Kdr*, *Mrc1* (encoding CD206), and *Stab1* in c2, and we employed CD206 as

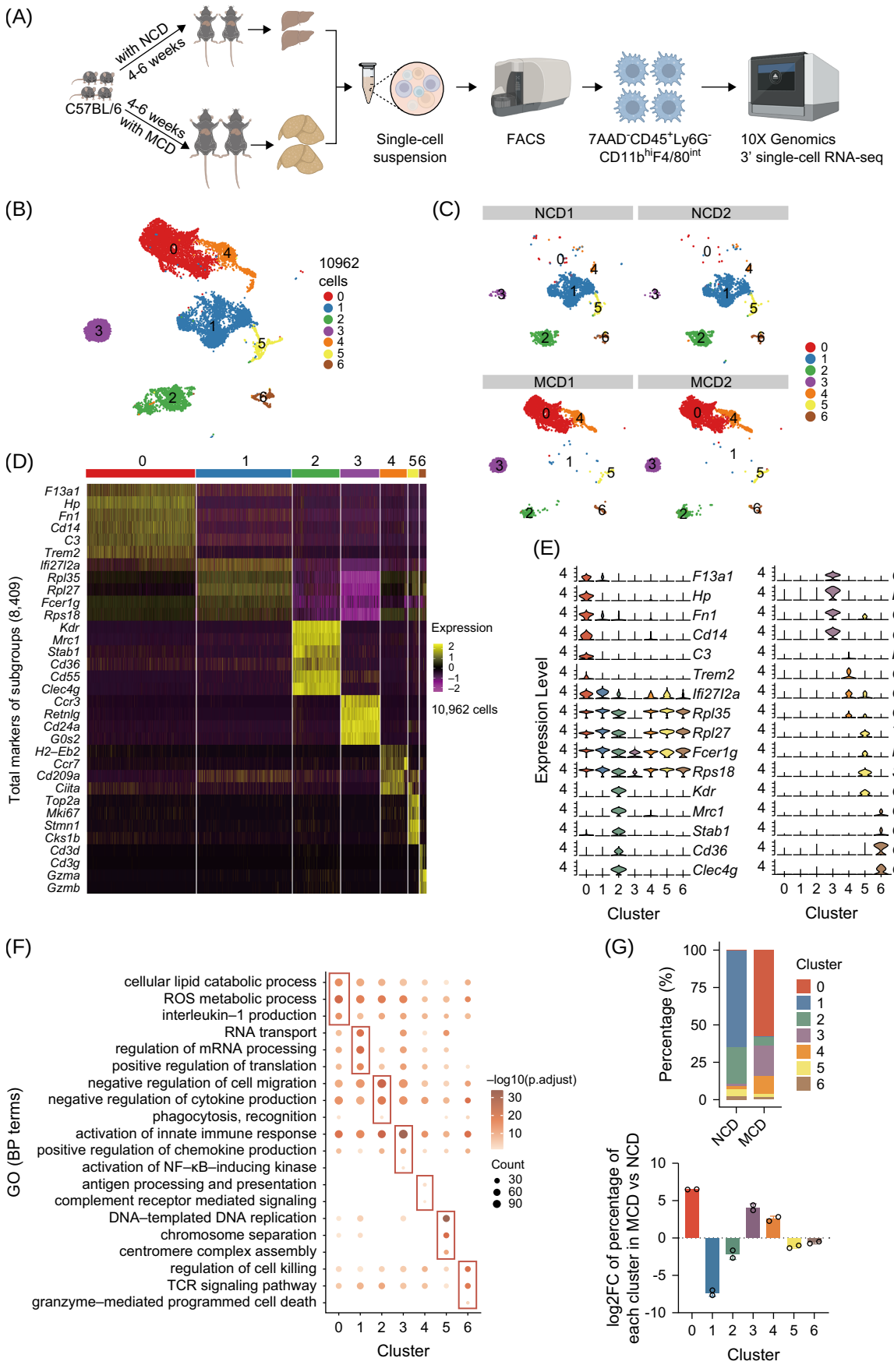
(A)
with NCD
4-6 weeks
C57BL/6
4-6 weeks
with MCD
Single-cell suspension
FACS
7AAD-CD45+Ly6G-
CD11bhiF4/80int
10X Genomics
3' single-cell RNA-seq
(B)
10962 cells
0
1
2
3
4
5
6
(C)
NCD1
NCD2
MCD1
MCD2
(D)
Total markers of subgroups (8,409)
F13a1
Hp
Fn1
Cd14
C3
Trem2
Ifi27l2a
Rpl35
Rpl27
Fcer1g
Rps18
Kdr
Mrc1
Stab1
Cd36
Cd55
Clec4g
Ccr3
Retnlg
Cd24a
G0s2
H2–Eb2
Ccr7
Cd209a
Ciita
Top2a
Mki67
Stmn1
Cks1b
Cd3d
Cd3g
Gzma
Gzmb
Expression
10,962 cells
(E)
Expression Level
Cluster
(F)
GO (BP terms)
cellular lipid catabolic process
ROS metabolic process
interleukin–1 production
RNA transport
regulation of mRNA processing
positive regulation of translation
negative regulation of cell migration
negative regulation of cytokine production
phagocytosis, recognition
activation of innate immune response
positive regulation of chemokine production
activation of NF–κB–inducing kinase
antigen processing and presentation
complement receptor mediated signaling
DNA–templated DNA replication
chromosome separation
centromere complex assembly
regulation of cell killing
TCR signaling pathway
granzyme–mediated programmed cell death
–log10(p.adjust)
Count
Cluster
(G)
Percentage (%)
NCD
MCD
log2FC of percentage of each cluster in MCD vs NCD
Cluster

FIGURE 1 scRNA-seq analysis of the MoMFs landscape in the liver of mice fed with NCD and MCD diets. (A) The experimental procedure of scRNA-seq of intrahepatic MoMFs in NCD-fed (NCD) and MCD-fed (MCD) mice. (B) Uniform manifold approximation and projection (UMAP) plot depicting clustering patterns of MoMFs from mouse liver. (C) UMAP plots displaying major subsets identified in NCD and MCD. (D, E) Heatmap (D) and violin plots (E) displaying the expression of representative marker genes of each cluster. (F) Dot plots depicting the enriched biological process (BP) terms for all markers identified in each MoMFs cluster. (G) The percentage (upper) and the magnitude (lower, expressed as log2FC) of 7 clusters among total MoMFs. Abbreviations: MCD, methionine/choline-deficient diet; MoMFs, monocyte-derived macrophages; NCD, normal control diet; scRNA-seq, single-cell RNA sequencing.

a definitive marker for this cluster in subsequent flow cytometric validation (Figure 2A). Flow cytometric analysis demonstrated that the proportion of $CD206^+$ MoMFs was significantly decreased in the livers of CDHFD-fed, MCD-fed, and HFD-fed mice compared with that in NCD-fed mice, consistent with the results of scRNA-seq analysis (Figure 2B). Histopathological examination by Hematoxylin and Eosin (H&E) staining confirmed the development of hepatic steatosis and inflammation in MCD-fed mice (Figure 2C). Notably, correlation analysis revealed a significant negative correlation between the proportion of $CD206^+$ MoMFs and the NAFLD activity score (NAS) in the livers of NCD-fed and MCD-fed mice, indicating that the reduction of this anti-inflammatory macrophage subset is closely associated with disease severity (Figure 2D).

Analysis of differentially expressed genes (DEGs) between MCD and NCD groups in c2 revealed 3481 upregulated and 1110 downregulated genes, notably including decreased expression of mitochondria-associated genes (Supplemental Figure S2A, http://links.lww.com/HC9/C281). GO and KEGG pathway enrichment analyses demonstrated significant upregulation of phagocytosis-related, autophagy-related, and apoptosis-related pathways (Figures 2E, F). Molecular characterization revealed decreased expression of mitochondria-associated genes concurrent with elevated expression of phagocytosis-related, autophagy-related, and apoptosis-related genes in the MCD group (Figure 2G). Further flow cytometry analysis confirmed increased lipid accumulation, impaired mitochondrial function, and elevated apoptosis in $CD206^+$ MoMFs from both CDHFD-fed and MCD-fed mice, suggesting that lipid overload drives mitochondrial dysfunction and promotes apoptosis in these cells (Figures 2H–J).

$CCR3^+$ (c3) MoMFs drive MASLD progression through lipid accumulation, oxidative stress, and CCL5-mediated recruitment

A distinctive MoMFs cluster (c3) was identified through scRNA-seq analysis, which showed prominent expression of *Ccr3*, *Retnlg*, *Cd24a*, and *G0s2* (Figure 3A). Flow cytometry validation confirmed a significant increase in $CCR3^+$ MoMFs in the livers of CDHFD-fed, MCD-fed, and HFD-fed mice compared with NCD-fed mice (Figure 3B). Importantly, the proportion of $CCR3^+$ MoMFs positively correlated with NAS (Figure 3C), suggesting their pathogenic contribution scales with disease severity. DEGs analysis of c3, coupled with GO and KEGG pathway enrichment, revealed upregulation of pathways related to immune response activation, lymphocyte chemotaxis, and oxidative stress in MCD-fed mice (Figure 3D and Supplemental Figure S2B, http://links.lww.com/HC9/C281). Specifically, genes involved in lipid metabolism and cell activation showed elevated expression (Figure 3E). Using flow cytometry, we observed markedly elevated CCL2 levels in c3 from CDHFD-fed mice, indicating enhanced pro-inflammatory responses (Figure 3F). Compared with the NCD group, CDHFD-fed and HFD-fed groups exhibited significantly enhanced BODIPY staining, suggesting markedly increased lipid accumulation; concurrently, ROS levels were significantly elevated in CDHFD-fed and MCD-fed groups, indicating intensified oxidative stress during MASLD progression (Figures 3G, H). These findings suggest that $CCR3^+$ MoMFs represent a pathogenic subset that contributes to MASLD progression through enhanced lipid accumulation, oxidative stress, and pro-inflammatory responses. Consistent with this notion, our prior work demonstrated that $CCR3^+$ MoMFs depletion via a neutralizing antibody significantly alleviated hepatic steatosis, lobular inflammation, and glucose intolerance in CDHFD-fed and MCD-fed murine models,[25] further supporting the pathogenic role of this subset in MASLD.

Given the significant expansion of $CCR3^+$ MoMFs in MASLD livers, we next investigated the mechanisms underlying their accumulation. Notably, proliferation and apoptosis levels of $CCR3^+$ MoMFs remained unchanged among the NCD-fed, CDHFD-fed, and HFD-fed groups (Supplemental Figures S2C, D, http://links.lww.com/HC9/C281), suggesting that the increased abundance of this subset is not attributable to local proliferation or reduced cell death. Consequently, we hypothesized that enhanced recruitment is the primary driver. To explore potential recruitment mechanisms, we analyzed publicly available scRNA-seq data (GSE212837) from healthy individuals and MASLD patients.[30] CellChat analysis revealed that macrophages actively interact with hepatocytes (Hep), endothelial cells (EC), cholangiocytes (Cholangio), monocyte/macrophages (Mono/Mac), and B cells in the liver through CCR3–CCL5 ligand–receptor pairs (Figure 3I). Moreover, analysis of a public mouse

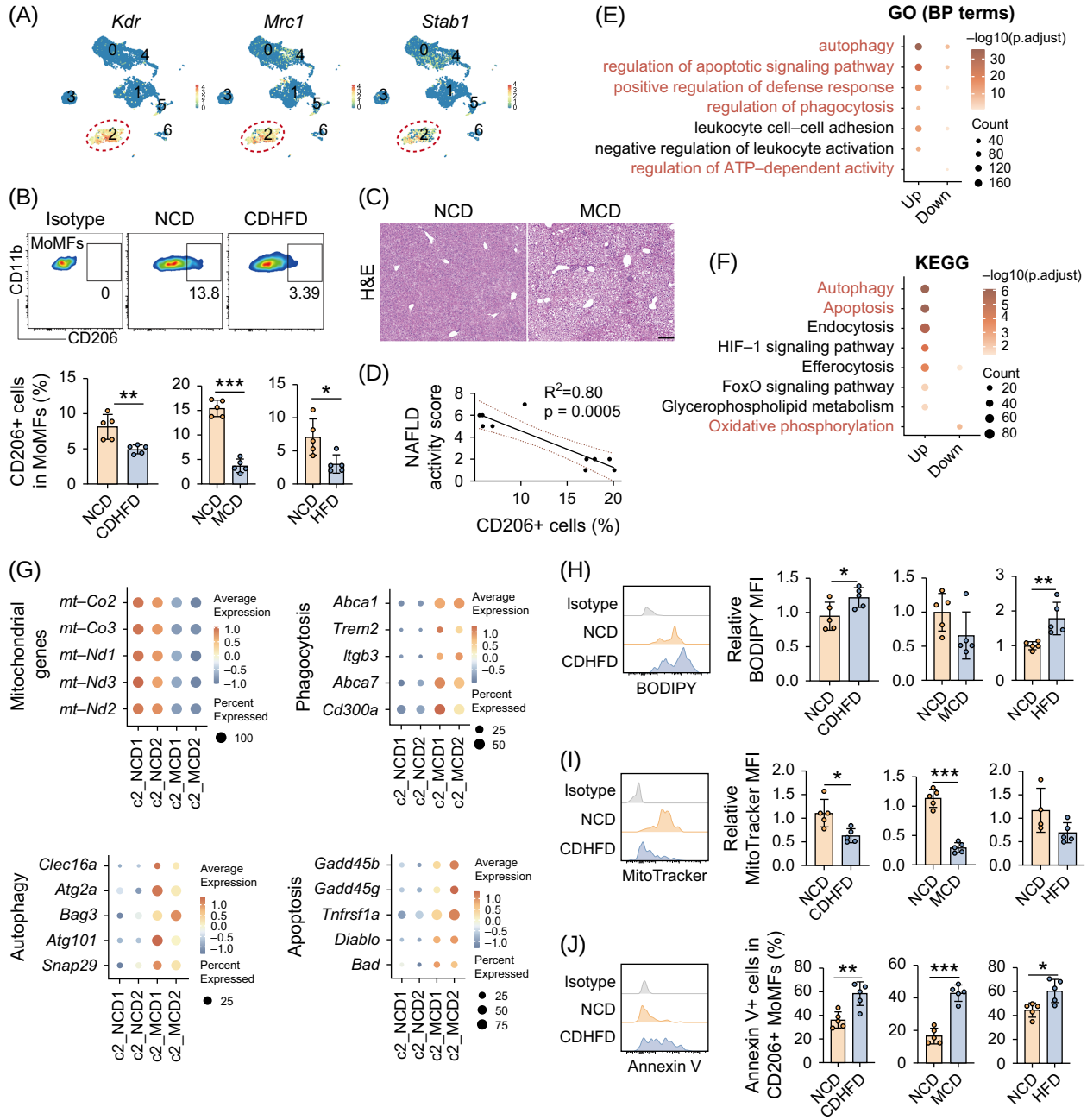

FIGURE 2 Lipid accumulation impairs mitochondrial function and promotes apoptosis in hepatic CD206$^+$ (c2) MoMFs. (A) Feature plots displaying the expression of *Kdr*, *Mrc1*, and *Stab1*. (B) Flow cytometry analysis showing CD206$^+$ MoMFs proportions among total MoMFs across NCD-fed, CDHFD-fed, MCD-fed, and HFD-fed mice, with representative plots (upper) and quantitative data (lower). (C) Representative images of H&E staining in liver paraffin sections. Scale bars, 200 μm. (D) Correlation between the proportion of CD206$^+$ MoMFs and the NAFLD activity score in the combined cohort of NCD-fed and MCD-fed mice. (E, F) Dot plots show the enriched GO (E) and KEGG (F) terms of DEGs in CD206$^+$ MoMFs between the NCD and MCD groups. Dot size denotes the enriched gene counts. The color bar denotes the adjusted *p*-value of enrichment. (G) Dot plots show the average expression levels of selected DEGs. Dot size denotes the percentage of expressed cells, and the color bar denotes scaled average expression. (H–J) Representative flow cytometry plots (left) and corresponding statistical analysis (right) of BODIPY (H), MitoTracker (I), and Annexin V (J) in CD206$^+$ MoMFs from NCD-fed, CDHFD-fed, MCD-fed, and HFD-fed mice. Abbreviations: CDHFD, choline-deficient high-fat diet; DEGs, differentially expressed genes; GO, Gene Ontology; HFD, high-fat diet; H&E, Hematoxylin and Eosin; KEGG, Kyoto Encyclopedia of Genes and Genomes; MCD, methionine/choline-deficient diet; MoMFs, monocyte-derived macrophages; NAFLD, nonalcoholic fatty liver disease; NCD, normal control diet.

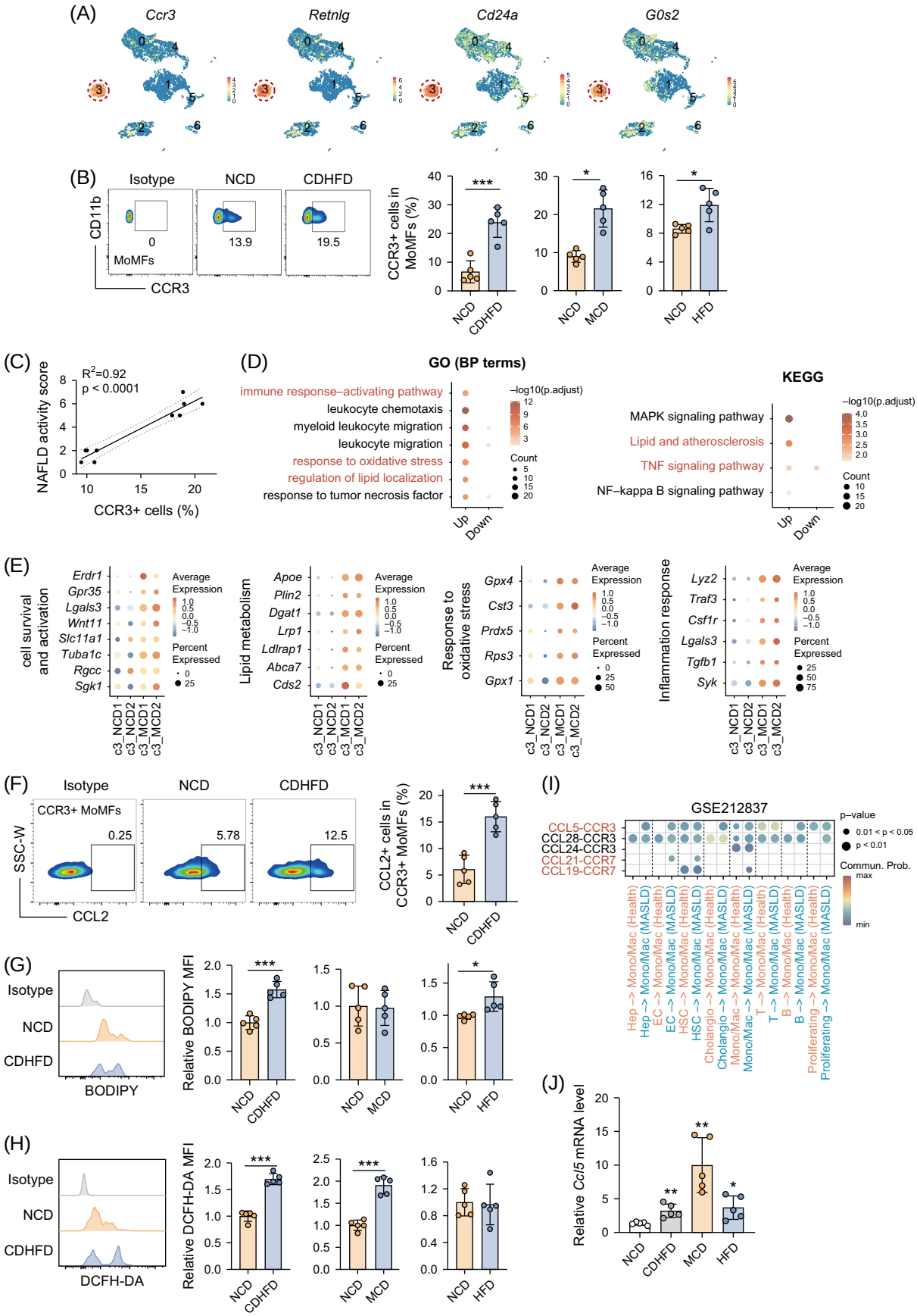
(A)
Ccr3
Retnlg
Cd24a
G0s2
(B)
Isotype
NCD
CDHFD
CD11b
CCR3
MoMFs
0
13.9
19.5
CCR3+ cells in MoMFs (%)
NCD
CDHFD
MCD
HFD
(C)
NAFLD activity score
R2=0.92
p < 0.0001
CCR3+ cells (%)
(D)
GO (BP terms)
immune response–activating pathway
leukocyte chemotaxis
myeloid leukocyte migration
leukocyte migration
response to oxidative stress
regulation of lipid localization
response to tumor necrosis factor
–log10(p.adjust)
Count
Up
Down
KEGG
MAPK signaling pathway
Lipid and atherosclerosis
TNF signaling pathway
NF–kappa B signaling pathway
(E)
cell survival and activation
Erdr1
Gpr35
Lgals3
Wnt11
Slc11a1
Tuba1c
Rgcc
Sgk1
Lipid metabolism
Apoe
Plin2
Dgat1
Lrp1
Ldlrap1
Abca7
Cds2
Response to oxidative stress
Gpx4
Cst3
Prdx5
Rps3
Gpx1
Inflammation response
Lyz2
Traf3
Csf1r
Lgals3
Tgfb1
Syk
Average Expression
Percent Expressed
c3_NCD1
c3_NCD2
c3_MCD1
c3_MCD2
(F)
Isotype
NCD
CDHFD
CCR3+ MoMFs
SSC-W
CCL2
0.25
5.78
12.5
CCL2+ cells in CCR3+ MoMFs (%)
(G)
Isotype
NCD
CDHFD
BODIPY
Relative BODIPY MFI
(H)
Isotype
NCD
CDHFD
DCFH-DA
Relative DCFH-DA MFI
(I)
GSE212837
CCL5-CCR3
CCL28-CCR3
CCL24-CCR3
CCL21-CCR7
CCL19-CCR7
p–value
Commun. Prob.
Hep –> Mono/Mac (Health)
Hep –> Mono/Mac (MASLD)
EC –> Mono/Mac (Health)
EC –> Mono/Mac (MASLD)
HSC –> Mono/Mac (Health)
HSC –> Mono/Mac (MASLD)
Cholangio –> Mono/Mac (Health)
Cholangio –> Mono/Mac (MASLD)
Mono/Mac –> Mono/Mac (Health)
Mono/Mac –> Mono/Mac (MASLD)
T –> Mono/Mac (Health)
T –> Mono/Mac (MASLD)
B –> Mono/Mac (Health)
B –> Mono/Mac (MASLD)
Proliferating –> Mono/Mac (Health)
Proliferating –> Mono/Mac (MASLD)
(J)
Relative Ccl5 mRNA level
NCD
CDHFD
MCD
HFD

FIGURE 3 CCR3$^+$ (c3) MoMFs promote MASLD progression via CCL5-mediated recruitment, leading to lipid accumulation and oxidative stress. (A) Feature plots displaying the expression of *Ccr3*, *Retnlg*, *Cd24a*, and *G0s2*. (B) Flow cytometry analysis showing CCR3$^+$ MoMFs proportions among total MoMFs across NCD-fed, CDHFD-fed, MCD-fed, and HFD-fed mice, with representative plots (left) and quantitative data (right). (C) Correlation between the proportion of CCR3$^+$ MoMFs and the NAFLD activity score in the combined cohort of NCD-fed and MCD-fed mice. (D) Dot plots show the enriched GO and KEGG terms of DEGs in CCR3$^+$ MoMFs between the NCD and MCD groups. Dot size denotes the enriched gene counts. The color bar denotes the adjusted *p*-value of enrichment. (E) Dot plots show the average expression levels of selected DEGs. Dot size denotes the percentage of expressed cells, and the color bar denotes scaled average expression. (F) Flow cytometry analysis showing the proportion of CCL2$^+$ cells among CCR3$^+$ MoMFs in NCD-fed and CDHFD-fed mice. (G, H) Flow cytometric analysis showing relative BODIPY MFI (G) and relative DCFH-DA MFI (H) in CCR3$^+$ MoMFs from NCD-fed, CDHFD-fed, MCD-fed, and HFD-fed mice. (I) Cell–cell interactions between liver cell subsets and Mono/Mac subsets in healthy controls and MASLD patients, analyzed using CellChat v2 based on GSE212837 data. Dot size indicates *p*-value significance, and color represents communication probability. (J) Relative mRNA levels of *Ccl5* in liver tissues of NCD-fed, CDHFD-fed, MCD-fed, and HFD-fed mice. Abbreviations: CDHFD, choline-deficient high-fat diet; DEGs, differentially expressed genes; GO, Gene Ontology; HFD, high-fat diet; H&E, Hematoxylin and Eosin; KEGG, Kyoto Encyclopedia of Genes and Genomes; MASLD, metabolic dysfunction–associated steatotic liver disease; MCD, methionine/choline-deficient diet; MoMFs, monocyte-derived macrophages; mRNA, messenger RNA; NAFLD, nonalcoholic fatty liver disease; NCD, normal control diet.

MASLD scRNA-seq dataset (GSE232182) also revealed enhanced CCL5–CCR3 interactions, with CCL5 secreted by hepatocytes, cholangiocytes, dendritic cells, and neutrophils, and CCR3 expressed on Mono/Mac (Supplemental Figure S2E, http://links.lww.com/HC9/C281), indicating a conserved role of this axis across species. Of note, cell clusters in the dataset were annotated based on canonical marker-gene expression; specifically, the Mono/Mac cluster was defined by high expression of *CD14*, *CD68*, *CSF1R*, and *FCGR3A*, which encompasses both liver-resident KCs and MoMFs, potentially introducing bias into the cell–cell interaction.

To validate this hypothesis, we conducted preliminary experimental validation using qPCR. Notably, *Ccl5* expression was significantly upregulated in the livers of CDHFD-fed, MCD-fed, and HFD-fed mice (Figure 3J), supporting the notion that elevated hepatic CCL5 promotes CCR3$^+$ MoMFs recruitment and amplifies the inflammatory response in MASLD progression.

CCL19/CCL21-recruited CCR7$^+$ (c4) MoMFs exacerbate MASLD pathogenesis through enhanced antigen presentation

To investigate the role of CCR7$^+$ MoMFs in MASLD progression, we first characterized this subset and examined its functional involvement in the disease. Feature plots analysis demonstrated elevated expression of multiple genes, including histocompatibility 2 class II antigen E beta2 (*H2-Eb2*), *Ccr7*, and *Cd209a* in c4 (Figure 4A). Subsequently, we identified CCR7 as a characteristic marker gene for this cluster and validated the presence of CCR7$^+$ MoMFs through flow cytometry analysis, which revealed an increased proportion of this cluster in CDHFD-fed, MCD-fed, and HFD-fed mice livers (Figure 4B). This expansion correlated with disease severity, as the proportion of CCR7$^+$ MoMFs showed a significant positive correlation with the NAS (Figure 4C). DEGs analysis followed by pathway enrichment analysis demonstrated upregulation of antigen presentation signaling pathways in the MCD group (Figures 4D, E, and Supplemental Figure S2F, http://links.lww.com/HC9/C281). Consistently, genes associated with antigen presentation exhibited heightened expression in c4 from the MCD group (Figure 4F). Flow cytometric analysis further confirmed elevated MHC-II levels in this cluster within CDHFD-fed, MCD-fed, and HFD-fed mouse livers (Figure 4G).

To further determine the functional contribution of CCR7$^+$ MoMFs, we administered a neutralizing antibody against CCR7 (MAB3477, R&D Systems) or an IgG2A isotype (clone 4B12, R&D Systems) to MCD-fed mice. This CCR7 intervention significantly reduced the intrahepatic abundance of CCR7$^+$ MoMFs (Figure 4H) and led to a concomitant improvement in disease parameters, including lower serum ALT and AST levels (Figures 4I, J), a lower NAS (Figures 4K, L), and attenuated fibrosis as assessed by Sirius red staining (Figures 4K, M). These results demonstrate that CCR7$^+$ MoMFs represent a distinct pathogenic subset critical for diet-induced steatohepatitis progression.

CellChat analysis of the public human dataset (GSE212837) revealed that Mono/Mac interact with HSCs and exhibit self-communication within the Mono/Mac population through the CCR7–CCL19 ligand–receptor pair, while communicating with endothelial cells and HSCs via CCR7–CCL21 (Figure 3I). qPCR analysis confirmed elevated expression levels of *Ccl19* and *Ccl21* in CDHFD-fed, MCD-fed, and HFD-fed mouse livers (Figure 4N). These findings suggest that during MASLD progression, CCR7$^+$ (c4) MoMFs are recruited to the liver via CCL19/CCL21 signaling and exert pathogenic effects through elevated antigen presentation activity.

For c5 and c6, feature plots showed that c5 highly expressed proliferation-related genes (including *Mki67*, *Top2a*, and *Stmn1*), while c6 expressed TCR function-related genes (such as *Cd3d*, *Gzma*, and *Gzmb*) (Figures 4O, R). Using Ki67 and CD3 as markers for c5 and c6, respectively, flow cytometry analysis revealed no significant differences in the proportions of these subsets among the NCD-fed, CDHFD-fed, MCD-fed, and HFD-fed groups (Figures 4P, S,

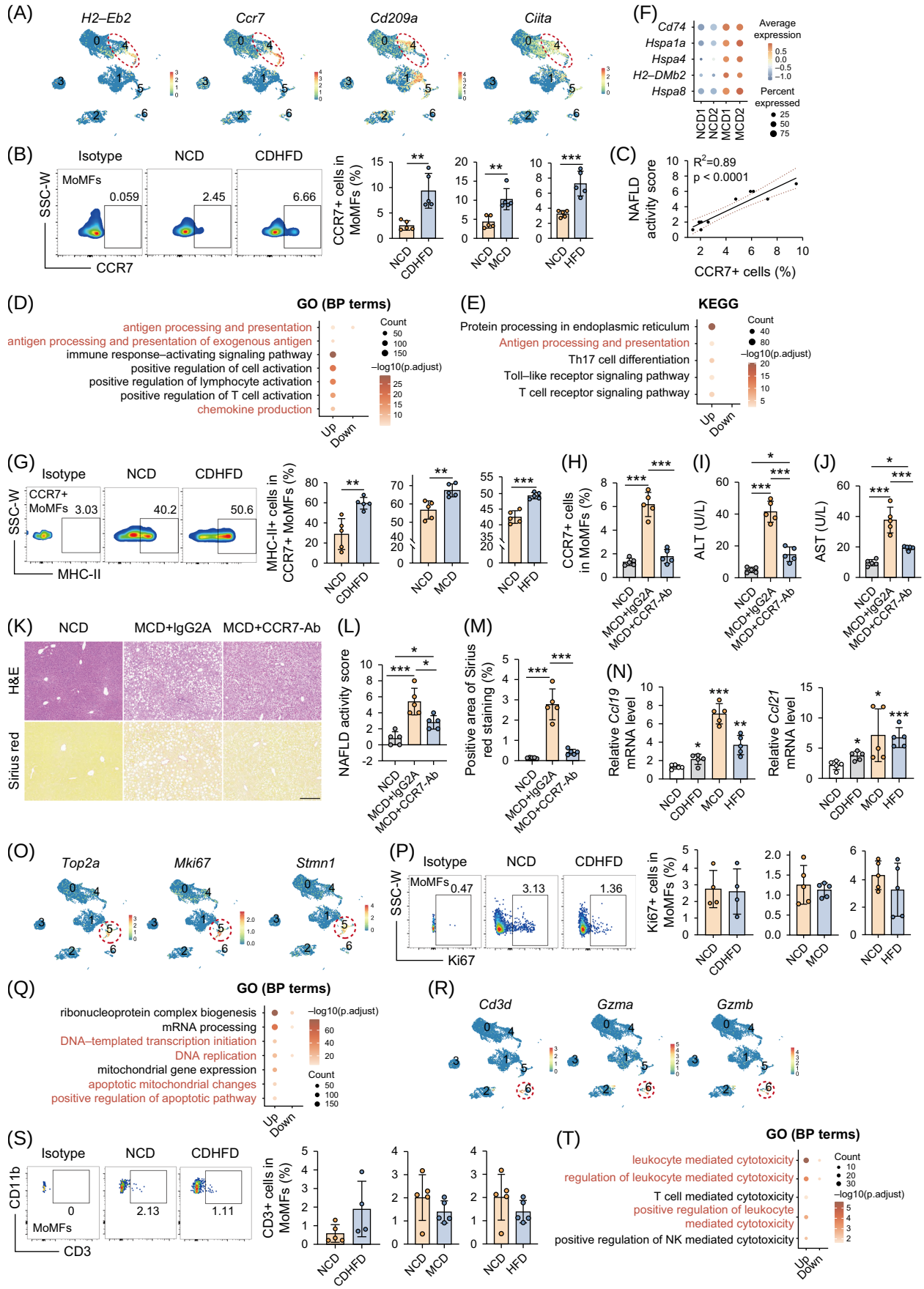
(A)
H2–Eb2
Ccr7
Cd209a
Ciita
(F)
Cd74
Hspa1a
Hspa4
H2–DMb2
Hspa8
Average expression
Percent expressed
NCD1
NCD2
MCD1
MCD2
(B)
Isotype
NCD
CDHFD
MoMFs
0.059
2.45
6.66
SSC-W
CCR7
CCR7+ cells in MoMFs (%)
NCD
CDHFD
MCD
HFD
(C)
NAFLD activity score
R²=0.89
p < 0.0001
CCR7+ cells (%)
(D)
GO (BP terms)
antigen processing and presentation
antigen processing and presentation of exogenous antigen
immune response–activating signaling pathway
positive regulation of cell activation
positive regulation of lymphocyte activation
positive regulation of T cell activation
chemokine production
Count
–log10(p.adjust)
Up
Down
(E)
KEGG
Protein processing in endoplasmic reticulum
Antigen processing and presentation
Th17 cell differentiation
Toll–like receptor signaling pathway
T cell receptor signaling pathway
(G)
Isotype
NCD
CDHFD
CCR7+ MoMFs
3.03
40.2
50.6
MHC-II
MHC-II+ cells in CCR7+ MoMFs (%)
(H)
CCR7+ cells in MoMFs (%)
(I)
ALT (U/L)
(J)
AST (U/L)
NCD
MCD+IgG2A
MCD+CCR7-Ab
(K)
NCD
MCD+IgG2A
MCD+CCR7-Ab
H&E
Sirius red
(L)
NAFLD activity score
(M)
Positive area of Sirius red staining (%)
(N)
Relative Ccl19 mRNA level
Relative Ccl21 mRNA level
(O)
Top2a
Mki67
Stmn1
(P)
Isotype
NCD
CDHFD
MoMFs
0.47
3.13
1.36
SSC-W
Ki67
Ki67+ cells in MoMFs (%)
(Q)
GO (BP terms)
ribonucleoprotein complex biogenesis
mRNA processing
DNA–templated transcription initiation
DNA replication
mitochondrial gene expression
apoptotic mitochondrial changes
positive regulation of apoptotic pathway
(R)
Cd3d
Gzma
Gzmb
(S)
Isotype
NCD
CDHFD
CD11b
MoMFs
0
2.13
1.11
CD3
CD3+ cells in MoMFs (%)
(T)
GO (BP terms)
leukocyte mediated cytotoxicity
regulation of leukocyte mediated cytotoxicity
T cell mediated cytotoxicity
positive regulation of leukocyte mediated cytotoxicity
positive regulation of NK mediated cytotoxicity

FIGURE 4 CCR7$^+$ (c4) MoMFs drive MASLD progression through enhanced antigen presentation and are recruited via the CCL19/CCL21 axis. (A) Feature plots displaying the expression of *H2-Eb2*, *Ccr7*, *Cd209a*, and *Ciita*. (B) Flow cytometry analysis showing CCR7$^+$ MoMFs proportions among total MoMFs across NCD-fed, CDHFD-fed, MCD-fed, and HFD-fed mice, with representative plots (left) and quantitative data (right). (C) Correlation between the proportion of CCR7$^+$ MoMFs and the NAFLD activity score in the combined cohort of NCD-fed and MCD-fed mice. (D, E) Dot plots show the enriched GO (D) and KEGG (E) terms of DEGs in CCR7$^+$ MoMFs between the NCD and MCD groups. Dot size denotes the enriched gene counts. The color bar denotes the adjusted *p*-value of enrichment. (F) Dot plots show the average expression levels of selected DEGs. Dot size denotes the percentage of expressed cells, and the color bar denotes scaled average expression. (G) Flow cytometry analysis showing MHC-II expression levels in CCR7$^+$ MoMFs across NCD-fed, CDHFD-fed, MCD-fed, and HFD-fed mice, with representative plots (left) and quantitative data (right). (H) Percentage of CCR7$^+$ cells among total intrahepatic MoMFs in mice. (I, J) Plasma ALT and AST levels in each group. (K–M) Representative images (K) and quantification of H&E staining (L) and Sirius red staining (M) in liver paraffin sections. Scale bars, 200 μm. (N) Relative mRNA levels of *Ccl19* (left) and *Ccl21* (right) in liver tissues of NCD-fed, CDHFD-fed, MCD-fed, and HFD-fed mice. (O) Feature plots displaying the expression of *Top2a*, *Mki67*, and *Stmn1*. (P) Flow cytometry analysis showing Ki67$^+$ MoMFs proportions among total MoMFs across NCD-fed, CDHFD-fed, MCD-fed, and HFD-fed mice, with representative plots (left) and quantitative data (right). (Q) Dot plots show the enriched GO terms of DEGs in Ki67$^+$ MoMFs between the NCD and MCD groups. Dot size denotes the enriched gene counts. The color bar denotes the adjusted *p*-value of enrichment. (R) Feature plots displaying the expression of *Cd3d*, *Gzma*, and *Gzmb*. (S) Flow cytometry analysis showing CD3$^+$ MoMFs proportions among total MoMFs across NCD-fed, CDHFD-fed, MCD-fed, and HFD-fed mice, with representative plots (left) and quantitative data (right). (T) Dot plots show the enriched GO terms of DEGs in CD3$^+$ MoMFs between the NCD and MCD groups. Dot size denotes the enriched gene counts. The color bar denotes the adjusted *p*-value of enrichment. Abbreviations: ALT, alanine transaminase; AST, aspartate aminotransferase; CDHFD, choline-deficient high-fat diet; HFD, high-fat diet; H&E, Hematoxylin and Eosin; MASLD, metabolic dysfunction–associated steatotic liver disease; MCD, methionine/choline-deficient diet; MoMFs, monocyte-derived macrophages; NAFLD, nonalcoholic fatty liver disease; NCD, normal control diet; UMAP, uniform manifold approximation and projection.

http://links.lww.com/HC9/C281). To further investigate the functional changes in these subsets during MASLD progression, we performed GO enrichment analysis on DEGs between the MCD and NCD groups. The results revealed that in c5, both DNA replication and apoptosis-related pathways were significantly upregulated in MCD-fed mice (Figure 4Q). Similarly, in c6, cytotoxicity-related pathways were significantly enriched in the MCD group (Figure 4T). These findings suggest that although c5 and c6 MoMFs maintain stable proportions during diet-induced steatohepatitis progression, they undergo functional reprogramming characterized by enhanced proliferative turnover and elevated cytotoxic activity, respectively.

CD14$^+$CCR2$^+$ (c0) MoMFs harbor functionally distinct subpopulations contributing to fibrosis, inflammation, lipid accumulation, and antigen presentation in MASLD

We focused on cluster 0, as it represented the cluster that exhibited the largest increase in proportion during MASLD progression. Feature plots indicated that this cluster was distinguished by high expression of genes such as *F13a1*, *Hp*, *Cd14*, and *Trem2*, with CD14 serving as a marker for this subset (Figure 5A). Flow cytometry results demonstrated a marked elevation in the proportion of CD14$^+$ MoMFs in CDHFD-fed, MCD-fed, and HFD-fed groups (Figure 5B). Furthermore, correlation analysis using the pooled data from NCD-fed and MCD-fed mice revealed a significant positive correlation between the proportion of CD14$^+$ MoMFs and NAS, underscoring the association of this subset with disease severity (Figure 5C). Notably, CCR2$^+$ MoMFs are traditionally regarded as the predominant subset of MoMFs in MASLD liver.[31] Consistent with this, our feature plot analysis revealed that *Ccr2* is also highly expressed in c0, particularly in the MASLD group, suggesting that CD14$^+$ (c0) MoMFs correspond to the classically defined CCR2$^+$ MoMFs (Figures 5A, D).

To explore the functional heterogeneity within this cluster, we further performed subclustering analysis, identifying seven distinct subclusters (sc0–sc6) (Supplemental Figure S2G, http://links.lww.com/HC9/C281). Feature plots and violin plots revealed that sc0 was enriched for pro-fibrotic genes, including matrix metallopeptidase 8 (*Mmp8*), selectin (*Sell*), and S100 calcium binding protein A10 (*S100a10*); sc2 exhibited high expression of pro-inflammatory genes such as G protein-coupled receptor 84 (*Gpr84*), C-type lectin domain family 5 member a (*Clec5a*), and *Tnf*; sc3 was characterized by high expression of genes involved in lipid accumulation, including triggering receptor expressed on myeloid cells-like 4 (*Treml4*), scavenger receptor *Cd36*, and triggering receptor expressed on myeloid cells 3 (*Trem3*); and sc4 showed high expression of genes related to antigen presentation (Figures 5E, F). In addition, three minor subpopulations showed unique signatures, including interferon response genes (sc1) and metabolic regulators (sc5 and sc6) (Supplemental Figure S2H, http://links.lww.com/HC9/C281). To validate these transcriptomic findings, flow cytometry analysis was performed, which revealed distinct alterations in CD14$^+$ MoMFs subpopulations across different dietary models. Compared with NCD controls, both MCD-fed and CDHFD-fed mice demonstrated significant increases in CD14$^+$Mmp8$^+$ (sc0, pro-fibrotic), CD14$^+$TNFα$^+$ (sc2, pro-inflammatory), CD14$^+$DCFH-DA$^+$ (sc2, oxidative stress), CD14$^+$CD36$^+$ (sc3, lipid-accumulating), and CD14$^+$MHC-II$^+$ (sc4, antigen-presenting) cell populations (Figures 5G–L). Moreover, CD14$^+$BODIPY$^+$ (sc3, lipid-accumulating) cells showed a specific increase in

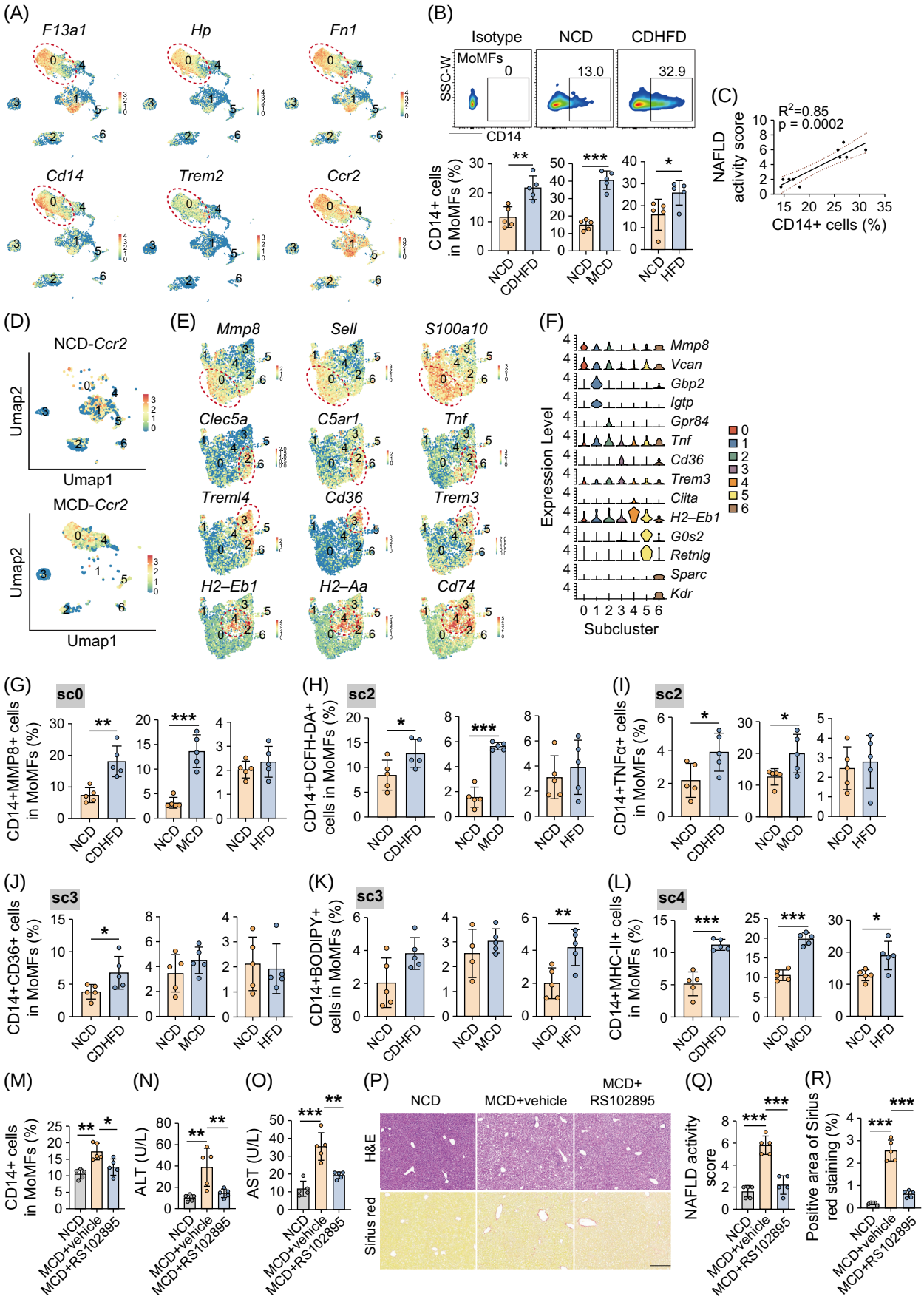
(A)
F13a1
Hp
Fn1
Cd14
Trem2
Ccr2
(B)
Isotype
NCD
CDHFD
MoMFs
SSC-W
CD14
13.0
32.9
CD14+ cells in MoMFs (%)
NCD
CDHFD
MCD
HFD
(C)
R2=0.85
p = 0.0002
NAFLD activity score
CD14+ cells (%)
(D)
NCD-Ccr2
MCD-Ccr2
Umap1
Umap2
(E)
Mmp8
Sell
S100a10
Clec5a
C5ar1
Tnf
Treml4
Cd36
Trem3
H2–Eb1
H2–Aa
Cd74
(F)
Mmp8
Vcan
Gbp2
Igtp
Gpr84
Tnf
Cd36
Trem3
Ciita
H2–Eb1
G0s2
Retnlg
Sparc
Kdr
Expression Level
Subcluster
(G)
sc0
CD14+MMP8+ cells in MoMFs (%)
(H)
sc2
CD14+DCFH-DA+ cells in MoMFs (%)
(I)
sc2
CD14+TNFα+ cells in MoMFs (%)
(J)
sc3
CD14+CD36+ cells in MoMFs (%)
(K)
sc3
CD14+BODIPY+ cells in MoMFs (%)
(L)
sc4
CD14+MHC-II+ cells in MoMFs (%)
(M)
CD14+ cells in MoMFs (%)
(N)
ALT (U/L)
(O)
AST (U/L)
(P)
NCD
MCD+vehicle
MCD+ RS102895
H&E
Sirius red
(Q)
NAFLD activity score
(R)
Positive area of Sirius red staining (%)

FIGURE 5 $CD14^+CCR2^+$ (c0) MoMFs represent a functionally heterogeneous population driving fibrosis, inflammation, and lipid accumulation in MASLD. (A) Feature plots displaying the expression of *F13a1*, *Hp*, *Fn1*, *Cd14*, *Trem2*, and *Ccr2*. (B) Flow cytometry analysis showing $CD14^+$ MoMFs proportions among total MoMFs across NCD-fed, CDHFD-fed, MCD-fed, and HFD-fed mice, with representative plots (upper) and quantitative data (lower). (C) Correlation between the proportion of $CD14^+$ MoMFs and the NAFLD activity score in the combined cohort of NCD-fed and MCD-fed mice. (D) Feature plots displaying the expression of Ccr2 in NCD and MCD. (E) Feature plots displaying the expression of *Mmp8*, *Sell*, *S100a10*, *Clec5a*, *C5ar1*, *Tnf*, *Treml4*, *Cd36*, *Trem3*, *H2-Eb1*, *H2-Aa*, and *Cd74*. (F) Violin plots displaying the expression of representative marker genes of each subcluster. (G–L) Statistical analysis of the percentages of $CD14^+MMP8^+$ (G), $CD14^+DCFH\text{-}DA^+$ (H), $CD14^+TNF\alpha^+$ (I), $CD14^+CD36^+$ (J), $CD14^+BODIPY^+$ (K), and $CD14^+MHC\text{-}II^+$ MoMFs (L) among the total MoMFs in NCD-fed, CDHFD-fed, MCD-fed, and HFD-fed mice. (M) Percentage of $CD14^+$ cells among total intrahepatic MoMFs in NCD, MCD+vehicle, and MCD+RS102895 groups. (N, O) Plasma ALT and AST levels in each group. (P–R) Representative images (P) and quantification of H&E staining (Q) and Sirius red staining (R) in liver paraffin sections. Scale bars, 200 μm. Abbreviations: ALT, alanine transaminase; AST, aspartate aminotransferase; CDHFD, choline-deficient high-fat diet; DEGs, differentially expressed genes; GO, Gene Ontology; HFD, high-fat diet; H&E, Hematoxylin and Eosin; KEGG, Kyoto Encyclopedia of Genes and Genomes; MASLD, metabolic dysfunction–associated steatotic liver disease; MCD, methionine/choline-deficient diet; MoMFs, monocyte-derived macrophages; mRNA, messenger RNA; NAFLD, nonalcoholic fatty liver disease; NCD, normal control diet.

HFD-fed mice (Figure 5K). Overall, our findings indicate that $CD14^+CCR2^+$ macrophages (c0) not only exhibit pro-inflammatory functions but also contribute to fibrosis, lipid accumulation, and antigen presentation.

To directly assess the pathogenic contribution of $CD14^+CCR2^+$ MoMFs to steatohepatitis progression, we treated MCD-fed mice with daily i.p. injections of the CCR2 antagonist RS102895 (5 mg/kg) or vehicle. This treatment significantly reduced the intrahepatic abundance of $CD14^+$ MoMFs (Figure 5M) and markedly ameliorated disease severity. Specifically, we observed reductions in serum ALT and AST levels (Figures 5N, O), improvement in NAS (Figures 5P, Q), and attenuation of fibrosis as assessed by Sirius red staining (Figures 5P, R). Together, these results indicate that the functionally diverse $CD14^+CCR2^+$ MoMFs play a critical pathogenic role in MASLD progression.

The basal cluster 1 (c1) is depleted during MASLD progression and acquires $CD14^+$ and $CCR7^+$ phenotypes under inflammatory stimulation in vitro

To investigate the fate and functional relevance of the dominant homeostatic cluster (c1) during MASLD, we performed integrated molecular and functional analyses. This cluster, most abundant in NCD livers (Figure 1G), exhibited high expression of ribosome-related genes (*Rpl27* and *Rpl15*), supporting its basal, non-inflammatory identity (Figure 6A). For precise identification, we defined c1 by the negative expression of other cluster markers (Figure 6B). Flow cytometry confirmed a significant reduction in c1 across multiple steatohepatitis models (Figure 6B). Moreover, its proportion negatively correlated with NAS, directly linking its depletion to disease severity (Figure 6C).

Intriguingly, CCR2 expression shifted from being primarily in c1 (NCD group) to predominantly in the inflammatory c0 in the MCD group, hinting at a possible phenotypic transition (Figures 5D, 6D). To formally test this plasticity, we performed pseudotime analysis on c0, c1, c4, and c5. The trajectory positioned c1 as the root state, with clear branching paths leading to c0 and c4/c5 lineages (Figures 6E, F). Notably, proliferative markers (c5) were also active early in the trajectory, suggesting proliferation may accompany this transition process (Figures 6E, F).

To test the plasticity and transition potential of c1 cells, we isolated them from the livers of NCD-fed mice (0 h) and cultured them for 24 hours with or without lipopolysaccharide (LPS) stimulation (100 ng/mL). Flow cytometry analysis revealed that after 24 hours of culture, isolated c1 cells acquired $CD14^+$ and $CCR7^+$ markers, even without LPS stimulation (Figures 6G, H). Notably, LPS treatment significantly enhanced this acquisition, with the LPS-stimulated group showing markedly higher proportions of $CD14^+$ and $CCR7^+$ MoMFs than the unstimulated group (Figures 6G, H). However, the proportion of $CCR3^+$ MoMFs showed no significant difference between the 2 groups (Figure 6I). These results suggest that c1 exhibits phenotypic plasticity, capable of acquiring $CD14^+$ and $CCR7^+$ markers under inflammatory stimulation in vitro.

To assess whether the 7 mouse clusters corresponded to human MASLD pathology, we analyzed human MASLD liver scRNA-seq data (GSE212837).[30] Our findings revealed that marker genes characterizing each mouse subpopulation were similarly expressed in human MASLD samples, with expression patterns between normal and MASLD patients mirroring the mouse subset dynamics (Figure 6J). These findings indicate that MASLD mouse model clusters are conserved in humans, suggesting their biological and clinical relevance in MASLD pathogenesis.

DISCUSSION

In summary, our comprehensive scRNA-seq analysis has advanced the understanding of MoMF heterogeneity in MASLD pathogenesis by revealing seven functionally distinct clusters with dynamic alterations during disease progression (Figure 7). These findings not only deepen our understanding of hepatic

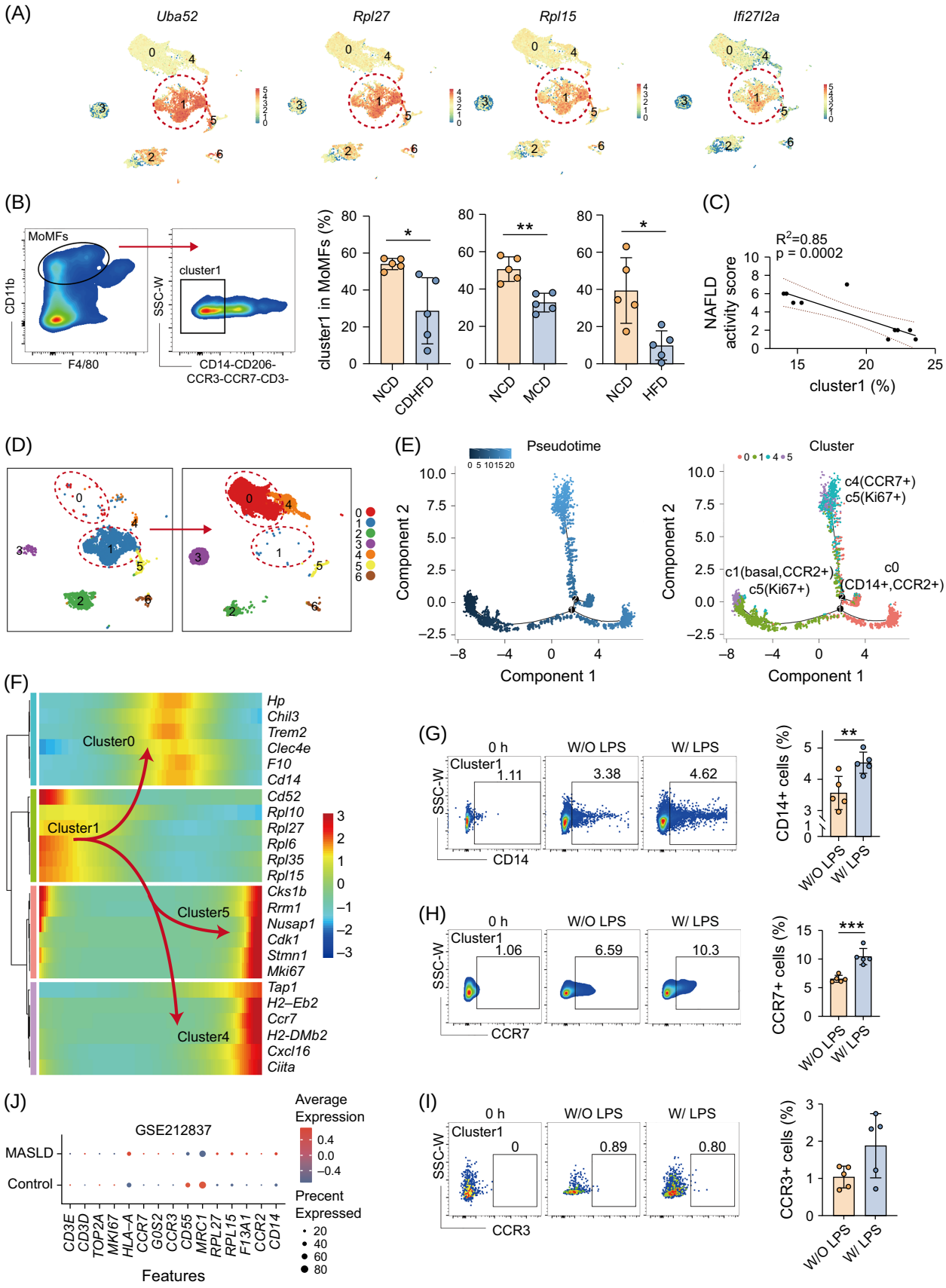

FIGURE 6 The basal cluster 1 (c1) is depleted during MASLD progression and acquires CD14$^+$ and CCR7$^+$ phenotypes under inflammatory stimulation in vitro. (A) Feature plots displaying the expression of *Uba52*, *Rpl27*, *Rpl15*, and *Ifi27l2a*. (B) The typical flow cytometry gating

strategy and statistical analysis of cluster 1 relative to total MoMFs in NCD-fed, CDHFD-fed, MCD-fed, and HFD-fed mice. (C) Correlation between the proportion of cluster 1 and the NAFLD activity score in the combined cohort of NCD-fed and MCD-fed mice. (D) UMAP plots displaying the major cellular subsets identified in the NCD and MCD groups. (E) Trajectory analysis of clusters 0, 1, 4, and 5 using Monocle 2. (F) Heatmap displaying gene expression dynamics across pseudotime for selected marker genes in clusters 0, 1, 4, and 5. (G–I) Flow cytometry analysis of CD14 (G), CCR7 (H), and CCR3 (I) expression in cluster 1 cells isolated from NCD-fed mouse liver, with or without LPS stimulation. (J) Dot plots depicting the expression of genes in liver macrophages derived from healthy and MASLD samples (GSE212837). Abbreviations: CDHFD, choline-deficient high-fat diet; HFD, high-fat diet; LPS, lipopolysaccharide; MASLD, metabolic dysfunction–associated steatotic liver disease; MCD, methionine/choline-deficient diet; MoMFs, monocyte-derived macrophages; NCD, normal control diet; UMAP, uniform manifold approximation and projection.

macrophage biology but also offer promising avenues for developing targeted immunomodulatory strategies to halt or reverse MASLD progression through selective manipulation of specific MoMFs subsets.

Multiple recent studies have characterized lipid-associated macrophages (LAMs) and monocyte-derived Kupffer cells (MoKCs) as key recruited macrophage populations in MASLD. We found that classical LAM markers (*Gpnmb*, *Trem2*, *Spp1*) were primarily expressed within the CD14$^+$ c0 cluster (Supplemental Figure S2I, http://links.lww.com/HC9/C281);[7,12,32] however, further subclustering of c0 revealed that these markers did not define a distinct, cohesive subpopulation, suggesting a more dispersed distribution of LAM-associated features among c0 MoMFs rather than a discrete LAM subset (Supplemental Figure S2J, http://links.lww.com/HC9/C281). In addition, canonical KC markers (*Clec4f*$^+$*Timd4*$^+$) and MoKCs (*Clec4f*$^+$*Timd4*$^-$) were rarely detected across all our MoMFs clusters (Supplemental Figure S2K, http://links.lww.com/HC9/C281),[33–35] consistent with the exclusion of resident KCs from our sorted MoMFs population (7AAD$^-$CD45$^+$Ly6G$^-$CD11b^{hi}F4/80^{int}). These observations indicate that while our c0 MoMFs share some transcriptomic overlap with LAMs, they likely represent a broader, functionally heterogeneous population rather than a dedicated LAMs lineage, and do not exhibit significant KC-like differentiation under the conditions studied.

While previous studies have primarily focused on CCR2$^+$ MoMFs as key mediators of inflammation through cytokine production and immune cell recruitment, we demonstrated that this population encompasses distinct subclusters with specialized functions in

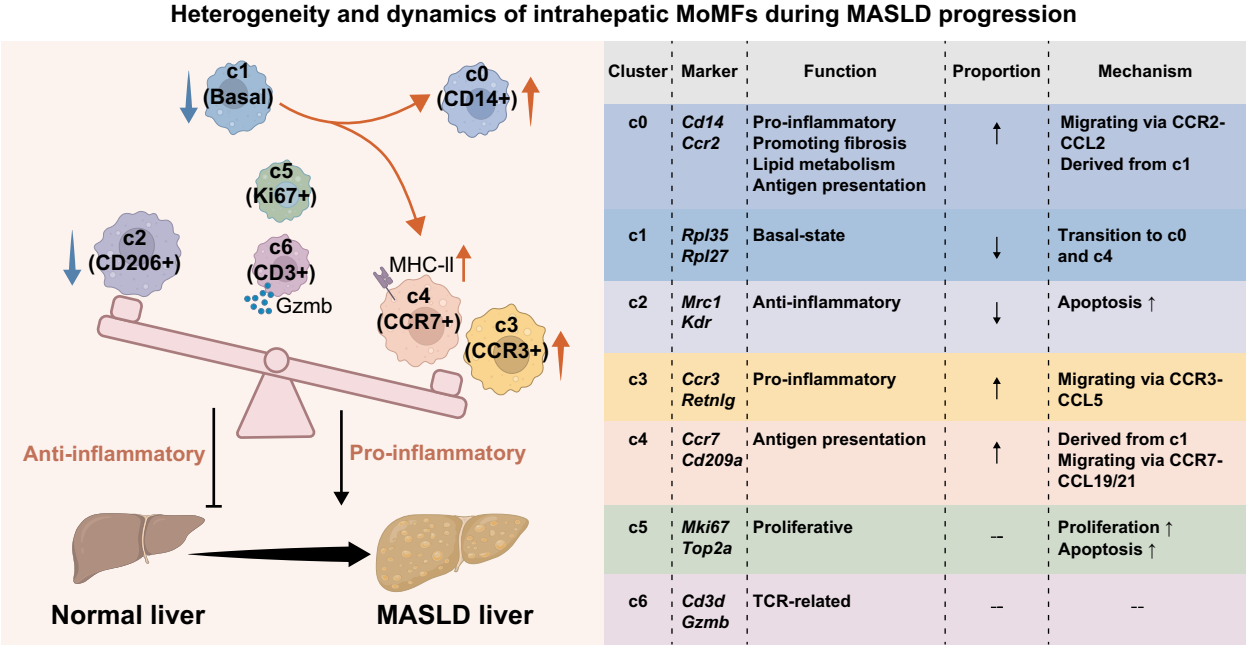

FIGURE 7 Heterogeneity and dynamics of intrahepatic MoMFs during MASLD progression. This scRNA-seq analysis delineated 7 distinct MoMFs clusters (c0–c6) in the liver with dynamic changes during steatohepatitis progression. CD14$^+$ (c0) MoMFs, the predominant CCR2$^+$ population, exhibited multifaceted functions beyond inflammation, including roles in fibrosis, lipid uptake, and antigen presentation. The basal cluster (c1) is depleted during MASLD progression and acquires CD14$^+$ and CCR7$^+$ phenotypes under inflammatory stimulation in vitro. Lipid overload drives mitochondrial dysfunction and apoptosis in CD206$^+$ (c2) MoMFs in MASLD. CCR3$^+$ (c3) MoMFs drive MASLD progression through lipid accumulation, oxidative stress, and CCL5-mediated recruitment. CCL19/CCL21-recruited CCR7$^+$ (c4) MoMFs exacerbate MASLD pathogenesis through enhanced antigen presentation. In addition, Ki67$^+$ (c5) proliferative and CD3$^+$ (c6) TCR-related MoMFs maintained stable proportions but exhibited functional alterations during MASLD. Abbreviations: MASLD, metabolic dysfunction–associated steatotic liver disease; MoMFs, monocyte-derived macrophages; scRNA-seq, single-cell RNA sequencing.

fibrosis, lipid droplet accumulation, and antigen presentation. This heterogeneity may explain the limited efficacy of therapies that broadly target CCR2/CCR5 recruitment in MASH patients. Our data suggest this approach may suppress disease-driving subsets while inadvertently limiting the pool of monocytes that could potentially adopt beneficial functions during resolution. Consequently, future work should focus on validating these pathogenic human MoMFs counterparts and identifying druggable targets within them to enable precise clinical intervention.

Our analysis identified a basal, ribosome-enriched MoMFs subset (c1), the relative abundance of which diminishes in MASLD. Pseudotime trajectory inference and in vitro phenotypic plasticity assays are consistent with a model in which c1 cells possess the capacity to transition into more inflammatory states under disease stress, potentially contributing to the expanded $CCR7^+$ (c4) and $CD14^+$ (c0) populations. However, we were unable to definitively establish this transition as a direct lineage commitment due to the absence of a unique surface marker for selective depletion or tracing of the c1 subset. Future studies employing more advanced techniques, such as single-cell multi-omics or the development of genetic tools that specifically target the c1 transcriptomic signature, will be essential to validate its precursor potential and elucidate its precise functional role within the hepatic microenvironment during MASLD progression.

The cell–cell communication analyses in this study utilized publicly available scRNA-seq data in which macrophages were identified using conventional markers (*CD14*, *CD68*, *CSF1R*, and *FCGR3A*), potentially mixing monocyte-derived and resident populations and thus representing an interpretive limitation. Nevertheless, the conserved upregulation of key chemokines such as *Ccl5*, *Ccl19*, and *Ccl21* across multiple dietary MASLD models provides initial experimental support for the predicted signaling axes. The CCL5–CCR3 axis has been implicated in regulating macrophage polarization and immune cell recruitment in multiple inflammatory contexts. Studies in cardiac remodeling demonstrated that CCL5 promotes M2 macrophage polarization through CCR3-dependent NF-κB activation.[36] Similarly, CCL5–CCR3 signaling facilitates Th2 cell differentiation, creating an immunosuppressive microenvironment.[37] The CCL21–CCR7 axis likewise plays a pivotal role in immune regulation. In rheumatoid arthritis, CCR7 upregulation in synovial macrophages promotes M1 polarization and Th17 cell differentiation, driving chronic inflammation.[38] These findings suggest that CCL5–CCR3 and CCL19/21-CCR7 signaling axes may serve as critical regulatory nodes orchestrating macrophage-immune cell crosstalk during MASLD progression, warranting further investigation as potential therapeutic targets.

Beyond transcriptomic conservation, our identified MoMFs subsets exhibit significant translational potential for therapeutic development. Crucially, we demonstrate that therapeutic targeting of specific subset markers (CCR7 or CCR2) ameliorates MASLD pathology. Notably, the clinical relevance of these targets is further supported by emerging evidence from human studies. The CCL24–CCR3 axis has emerged as a druggable target; human NASH patients show elevated CCL24 and CCR3 expression in liver biopsies and blood samples, and the anti-CCL24 monoclonal antibody CM-101 significantly attenuated liver fibrosis and NAFLD activity scores in 3 experimental models,[39] demonstrating the druggability of this pathway. Most encouragingly, therapeutic targeting of CCR7 has advanced to clinical development. CAP-100, a humanized anti-CCR7 monoclonal antibody (IgG1), specifically neutralizes CCR7 ligand-binding and signaling, inhibiting CCR7-mediated migration, extravasation, and survival.[40] These clinical developments collectively validate the translational significance of our mouse-derived MoMFs subsets, highlighting $CCR3^+$ and $CCR7^+$ populations as promising therapeutic targets for human MASLD.

Recent work by Guo et al.[41] elegantly dissected how the Notch–RBPJ signaling axis governs monocyte fate determination in MASLD. However, our study focuses on the functional heterogeneity of MoMFs within the steatotic liver microenvironment. We identify new subsets such as $CCR3^+$ and $CCR7^+$ MoMFs and dissect the multifunctional spectrum of $CCR2^+$ macrophages. Moreover, we observe that a basal resident MoMFs population exhibits phenotypic plasticity, pointing to local adaptations that may contribute to macrophage diversity alongside bone marrow recruitment. These findings provide a complementary, cell-state-centered perspective that extends our understanding of macrophage roles in MASLD pathogenesis.

While our findings advance MoMFs' biology understanding, several limitations should be acknowledged. First, scRNA-seq provides transcriptional snapshots that may miss transient states and lack spatial context; thus, the tissue localization of the identified macrophage subsets remains undefined, which could be addressed by spatial transcriptomics. Second, our study was conducted exclusively in male mice, and validation in female animals and alternative disease models is needed to establish broader clinical relevance. Third, functional contributions of each subset require precise definition through selective depletion or manipulation studies.

DATA AVAILABILITY STATEMENT

Raw data of scRNA-seq have been deposited at GEO as GSE295950 (reviewer token: ohopseeqzbwlban). The above data are publicly available as of the date of

publication. All data reported in this paper will be shared by the lead contact upon request.

FUNDING INFORMATION

Grants from the National Natural Science Foundation of China (82370578 and 82270606), Natural Science Foundation of Beijing Municipality (No. 7232034), and the Youth Beijing Scholar (No. 035) supported this work.

CONFLICTS OF INTEREST

The authors have no conflicts to report.

REFERENCES

1. Chen H, Zhan Y, Zhang J, Cheng S, Zhou Y, Chen L, et al. The global, regional, and national burden and trends of NAFLD in 204 countries and territories: An analysis from Global Burden of Disease 2019. JMIR Public Health Surveill. 2022;8:e34809.
2. Younossi ZM. Non-alcoholic fatty liver disease—A global public health perspective. J Hepatol. 2019;70:531–44.
3. Malhi H, Brown RS, Lim JK, Reau N, Tapper EB, Wong CC-L, et al. Precipitous changes in nomenclature and definitions—NAFLD becomes SLD: Implications for and expectations of AASLD journals. Hepatol Commun. 2023;7:e0318.
4. Yeh MM, Brunt EM. Pathological features of fatty liver disease. Gastroenterology. 2014;147:754–64.
5. Wang C, Ma C, Gong L, Guo Y, Fu K, Zhang Y, et al. Macrophage polarization and its role in liver disease. Front Immunol. 2021;12:803037.
6. Krenkel O, Tacke F. Liver macrophages in tissue homeostasis and disease. Nat Rev Immunol. 2017;17:306–21.
7. Daemen S, Gainullina A, Kalugotla G, He L, Chan MM, Beals JW, et al. Dynamic shifts in the composition of resident and recruited macrophages influence tissue remodeling in NASH. Cell Rep. 2021;34:108626.
8. Guillot A, Tacke F. Spatial dimension of macrophage heterogeneity in liver diseases. eGastroenterology. 2023;1:e000003.
9. Feng D, Guan Y, Wang Y, Maccioni L, Mackowiak B, Gao B. Characterisation of macrophages in healthy and diseased livers in mice: Identification of necrotic lesion-associated macrophages. eGastroenterology. 2025;3:e100189.
10. Krenkel O, Puengel T, Govaere O, Abdallah AT, Mossanen JC, Kohlhepp M, et al. Therapeutic inhibition of inflammatory monocyte recruitment reduces steatohepatitis and liver fibrosis. Hepatology. 2018;67:1270–83.
11. Ratziu V, Sanyal A, Harrison SA, Wong VW-S, Francque S, Goodman Z, et al. Cenicriviroc treatment for adults with nonalcoholic steatohepatitis and fibrosis: Final analysis of the phase 2b CENTAUR study. Hepatology. 2020;72:892.
12. Jaitin DA, Adlung L, Thaiss CA, Weiner A, Li B, Descamps H, et al. Lipid-associated macrophages control metabolic homeostasis in a Trem2-dependent manner. Cell. 2019;178:686–698.e14.
13. Xiong X, Kuang H, Ansari S, Liu T, Gong J, Wang S, et al. Landscape of intercellular crosstalk in healthy and NASH liver revealed by single-cell secretome gene analysis. Mol Cell. 2019;75:644–660.e5.
14. Wang Y, Zhang W, Li Z, Liu Y, Tan J, Yin H, et al. METTL14 downregulation drives S100A4+ monocyte-derived macrophages via MyD88/NF-κB pathway to promote MAFLD progression. Signal Transduct Target Ther. 2024;9:91.
15. Papalexi E, Satija R. Single-cell RNA sequencing to explore immune cell heterogeneity. Nat Rev Immunol. 2018;18:35–45.
16. Shi W, Wang Y, Zhang C, Jin H, Zeng Z, Wei L, et al. Isolation and purification of immune cells from the liver. Int Immunopharmacol. 2020;85:106632.
17. Pei G, Yao Y, Yang Q, Wang M, Wang Y, Wu J, et al. Lymphangiogenesis in kidney and lymph node mediates renal inflammation and fibrosis. Sci Adv. 2019;5:eaaw5075.
18. Liu J, Cheng Y, Zhang X, Chen Y, Zhu H, Chen K, et al. Glycosyltransferase Extl1 promotes CCR7-mediated dendritic cell migration to restrain infection and autoimmunity. Cell Rep. 2023;42:111991.
19. Liu S, Zhou Y, Li G, Zhu B, Wu F, Zhou J, et al. PLAUR^{+} neutrophils drive anti-PD-1 therapy resistance in patients with hepatocellular carcinoma by shaping an immunosuppressive microenvironment. Adv Sci. 2025;12:e07167.
20. Cai Y, Lu Z, Chen C, Zhu Y, Chen Z, Wu Z, et al. An atlas of genetic effects on cellular composition of the tumor microenvironment. Nat Immunol. 2024;25:1959–75.
21. Seidman JS, Troutman TD, Sakai M, Gola A, Spann NJ, Bennett H, et al. Niche-specific reprogramming of epigenetic landscapes drives myeloid cell diversity in nonalcoholic steatohepatitis. Immunity. 2020;52:1057–74.e7.
22. Moreno-Fernandez ME, Miraldi ER, Divanovic S. Not chopped liver—A careful, fate-mapping study of macrophages in NASH. Cell Metab. 2020;32:328–30.
23. Vonderlin J, Chavakis T, Sieweke M, Tacke F. The multifaceted roles of macrophages in NAFLD pathogenesis. Cell Mol Gastroenterol Hepatol. 2023;15:1311–24.
24. Rantakari P, Patten DA, Valtonen J, Karikoski M, Gerke H, Dawes H, et al. Stabilin-1 expression defines a subset of macrophages that mediate tissue homeostasis and prevent fibrosis in chronic liver injury. Proc Natl Acad Sci U S A. 2016;113:9298–303.
25. Sun G, Wang Y, Yang L, Zhang Z, Zhao Y, Shen Z, et al. Rebalancing liver-infiltrating CCR3+ and CD206+ monocytes improves diet-induced NAFLD. Cell Rep. 2023;42:112753.
26. Xuan W, Qu Q, Zheng B, Xiong S, Fan G-H. The chemotaxis of M1 and M2 macrophages is regulated by different chemokines. J Leukoc Biol. 2015;97:61–9.
27. MacParland SA, Liu JC, Ma X-Z, Innes BT, Bartczak AM, Gage BK, et al. Single cell RNA sequencing of human liver reveals distinct intrahepatic macrophage populations. Nat Commun. 2018;9:4383.
28. Rodriguez-Cruz A, Vesin D, Ramon-Luing L, Zuñiga J, Quesniaux VFJ, Ryffel B, et al. Macrophages deliver proinflammatory cytokines by a CD3- and transmembrane TNF-dependent pathway and are increased at the BCG-infection site. Front Immunol. 2019;10:2550.
29. Wang C, Zai W, Zhao K, Li Y, Shi B, Wu M, et al. Potential role of liver-resident CD3+ macrophages in HBV clearance in a mouse hepatitis B model. JHEP Rep. 2025;7:101323.
30. Wang S, Li K, Pickholz E, Dobie R, Matchett KP, Henderson NC, et al. An autocrine signaling circuit in hepatic stellate cells underlies advanced fibrosis in non-alcoholic steatohepatitis. Sci Transl Med. 2023;15:eadd3949.
31. Kazankov K, Jørgensen SMD, Thomsen KL, Møller HJ, Vilstrup H, George J, et al. The role of macrophages in nonalcoholic fatty liver disease and nonalcoholic steatohepatitis. Nat Rev Gastroenterol Hepatol. 2019;16:145–59.
32. Hendrikx T, Porsch F, Kiss MG, Rajcic D, Papac-Miličević N, Hoebinger C, et al. Soluble TREM2 levels reflect the recruitment and expansion of TREM2+ macrophages that localize to fibrotic areas and limit NASH. J Hepatol. 2022;77:1373–85.
33. Barreby E, Chen P, Aouadi M. Macrophage functional diversity in NAFLD—More than inflammation. Nat Rev Endocrinol. 2022;18:461–72.
34. Lefere S, Tacke F. Macrophages in obesity and non-alcoholic fatty liver disease: Crosstalk with metabolism. JHEP Rep. 2019;1:30–43.

35. Bonnardel J, T'Jonck W, Gaublomme D, Browaeys R, Scott CL, Martens L, et al. Stellate cells, hepatocytes, and endothelial cells imprint the Kupffer cell identity on monocytes colonizing the liver macrophage niche. Immunity. 2019;51:638–654.e9.
36. Lv S, Zhou M, Li T, Zeng Z, Yan Z, Hou Y, et al. CCL5 promotes angiotensin II-induced cardiac remodeling through regulation of platelet-driven M2 macrophage polarization. Theranostics. 2026;16:689–711.
37. Zhang Q, Qin J, Zhong L, Gong L, Zhang B, Zhang Y, et al. CCL5-mediated Th2 immune polarization promotes metastasis in luminal breast cancer. Cancer Res. 2015;75:4312–21.
38. Han L, Zhang L. CCL21/CCR7 axis as a therapeutic target for autoimmune diseases. Int Immunopharmacol. 2023;121: 110431.
39. Segal-Salto M, Barashi N, Katav A, Edelshtein V, Aharon A, Hashmueli S, et al. A blocking monoclonal antibody to CCL24 alleviates liver fibrosis and inflammation in experimental models of liver damage. JHEP Rep. 2020;2:100064.
40. Cuesta-Mateos C, Juárez-Sánchez R, Mateu-Albero T, Loscertales J, Mol W, Terrón F, et al. Targeting cancer homing into the lymph node with a novel anti-CCR7 therapeutic antibody: The paradigm of CLL. mAbs. 2021;13:1917484.
41. Guo W, Li Z, Anagnostopoulos G, Kong WT, Zhang S, Chakarov S, et al. Notch signaling regulates macrophage-mediated inflammation in metabolic dysfunction-associated steatotic liver disease. Immunity. 2024;57:2310–327.e6.

How to cite this article: Xu H, Yang L, Fang P, Sun J, Zhong X, Deng W, et al. Single-cell profiling reveals hepatic monocyte-derived macrophages heterogeneity during steatotic liver disease. Hepatol Commun. 2026;10:e0928. https://doi.org/10.1097/HC9.0000000000000928